Light Metals 2011 *Edited by: Stephen J. Lindsay*
TMS (The Minerals, Metals & Materials Society), 2011

SOME ASPECTS OF HEAT TRANSFER BETWEEN BATH AND SIDELEDGE IN ALUMINIUM REDUCTION CELLS

Asbjørn Solheim

SINTEF Materials and Chemistry; P.O. Box 4760 Sluppen, NO-7465 Trondheim, Norway

Key words: Bath; sideledge; heat transfer; superheat

Abstract

A literature review concerning the heat transfer coefficient between bath and sideledge (h) is given. Normally, the heat transfer is controlled mainly by the circulating bath motion due to gas drainage into the peripheral channel. After the introduction of slotted anodes that direct the gas towards the centre channel, it is likely that h will be determined by natural convection in some cases, and an equation is suggested to take this into account. The coupling between heat and mass transfer during melting and freezing of sideledge was studied in a numerical model involving multicomponent diffusion. During freezing, the concentration of bath components other than cryolite is higher at the ledge surface than in the bulk of the bath. The surface temperature of the ledge varies with the rate of freezing and melting, in such a way that the variation of the ledge thickness becomes slower than thought earlier.

Introduction

No other material than frozen cryolite can withstand the harsh conditions encountered in aluminium reduction cells, comprising oxidizing gases, a cryolite-based electrolyte (bath) kept at high temperature, and reducing molten or dissolved metal. To maintain such a frozen layer, the cells are designed to have a high heat flux through the sides. Besides protecting the sidelining, the freeze (sideledge, ledge) acts as a thermal buffer by freezing and melting.

The heat transported from the bath to the surface of the ledge is commonly calculated by the well-known equation

$$q = h \cdot (T_b - T_{liq}) \qquad [Wm^{-2}] \qquad (1)$$

where h is the heat transfer coefficient [$Wm^{-2}K^{-1}$] and T is the temperature; subscripts "b" and "liq" indicate the bulk of the bath and the liquidus, respectively. Eq. (1) explicitly assumes that the ledge surface temperature is equal to the liquidus temperature of the bulk of the electrolyte. The heat transfer coefficient can be controlled by forced convection, or – probably less recognized – by natural convection.

When calculating the total heat flow from the bath and out through the sides, it becomes obvious that the bath heat transfer coefficient represents only a minor part of the total heat resistance between the bath and the surroundings. Therefore, it can be argued that the average value of the heat transfer coefficient between the bath and the sideledge is not important for the average ledge thickness. However, the average heat transfer coefficient determines the average superheat, and local variations in the heat transfer coefficient (or superheat) may give local variations in the ledge thickness. The main resistances against heat flow are represented by conduction through the sideledge and by heat transfer (convection and radiation) between the potshell and its surroundings. To ensure a stable and thick enough sideledge, cooling ribs at the potshell could be a solution in some cases.

The bath heat transfer coefficient determines the rate of melting or freezing of the sideledge in periods when the cell is not at thermal balance, *i.e.*, during melting or freezing of sideledge. If the heat flux from bath to sideledge is different from the heat flux into the ledge, that difference is used for melting or freezing. However, the sideledge has a chemical composition that is different from the bath. Therefore, melting or freezing of sideledge must involve mass transfer between the bath/sideledge interface and the bulk of the bath, and consequently, the bath composition facing the ledge is not equal to the bulk composition. This means that the assumption of a ledge surface temperature equal to the liquidus temperature of the bulk bath is strictly true only when the sideledge is at thermal balance, *i.e.*, when neither freezing nor melting takes place.

The present paper provides a general description of heat transfer between bath and sideledge. The main topic, however, is the problem of predicting the rate of freezing or melting in a situation with coupled heat and mass transfer.

Heat Transfer at Steady State

Literature Data

Some literature values [1-13] for the heat transfer coefficient are given in Figure 1. The figure shows a considerable scatter, partly because the data were obtained by a variety of methods, including calculation and modelling, experiments in physical models, and measurements in cryolitic melts. Newer data, from the 1980s on, show higher values than older data, which is harder to explain. One fact that to be pointed out however, is that modelling, as well as interpretation of data obtained in physical models, requires a correct value for the thermal conductivity of the bath. New data on the thermal conductivity was published by Khokhlov *et al.* [13] in 1998. Their data showed a more than two-fold increase above earlier values. In fact, the heat transfer coefficients given by Khokhlov *et al.* [13] (item 13 in Figure 1) emerged from a re-interpretation of Solheim and Thonstad's experimental data obtained in a physical model [7]; the original interpretation is

shown as item 7 in Figure 1. The semi-empirical correlations given by Khoklov *et al.* [13] were later fully confirmed by CFD modelling [14]. It can, therefore, be assumed that the heat transfer coefficient between bath and sideledge is in the order of 1000 $Wm^{-2}K^{-1}$.

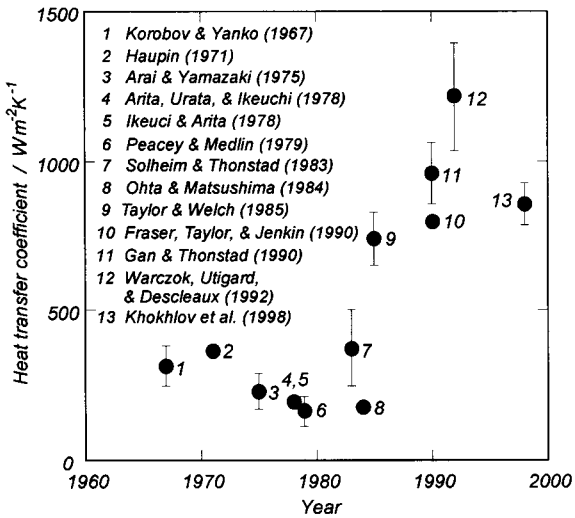

Figure 1. Literature values of the heat transfer coefficient between bath and sideledge in aluminium cells.

Functional Dependencies

Forced Convection. The heat transfer coefficient is normally thought to be governed by gas induced circulation in the peripheral channel. The intensity of the convection increases with increasing rate of gas drainage into the channel (G, $[m^3s^{-1}m^{-1}]$), increasing anode immersion depth (H, [m]) and decreasing anode-ledge distance (L, [m]). Based on Solheim and Thonstad's [7] data for different part of the ledge, later re-interpreted by Khokhlov *et al.* [13], the following expression for calculating the average heat transfer coefficient can be suggested,

$$h = 31480\left(\frac{GH}{L}\right)^{0.46} \quad [Wm^{-2}K^{-1}] \qquad (2)$$

For an anode with dimensions 1.6 x 0.7 m and carrying 10 kA at 960 °C, the rate of gas drainage will be $G = 5.7 \cdot 10^{-4}$ $m^3s^{-1}m^{-1}$, provided that the drainage is uniformly distributed along the anode periphery. Taking H = 0.15 m and L = 0.20 m, the heat transfer coefficient becomes 888 $Wm^{-2}K^{-1}$. This number may be somewhat higher due to magnetohydrodynamic flow along the channel [7]; on the other hand, it is known that more gas is drained into the centre channel than into the side channel. The latter is particularly important when using drained cathodes.

Natural Convection. Natural (free) convection is set up when there are density differences between the liquid facing the surface and the bulk. The density difference may be due to temperature gradients, gradients in chemical composition, or both. The following relationship was derived by Churchill and Chu (recommended in Welty *et al.*[15]),

$$Nu = \left\{0.825 + \frac{0.387 \cdot Ra^{1/6}}{\left[1+(0.492/Pr)^{9/16}\right]^{4/9}}\right\}^2 \qquad (3)$$

where Nu is the dimensionless Nusselt number, Ra is the Raleigh number, and Pr is the Prandtl number,

$$Nu = \frac{hL}{\lambda}; \quad Pr = \frac{\mu C_p}{\lambda}; \quad Ra = \frac{\rho \Delta\rho g L^3 C_p}{\lambda \mu} \qquad (4)$$

where L is the characteristic length (the bath height, taken to be 0.2 m), λ is the thermal conductivity of the bath, μ is the dynamic viscosity, C_p is the heat capacity of molten cryolite, ρ is the density of the bath, and $\Delta\rho$ is the density difference between the ledge surface and the bulk (calculated as $0.927 \cdot \Delta T$ [19]). The numerical values for the physical data used in the present paper can be found in Table I in the following.

The transition from laminar to turbulent natural convection normally takes place at $Ra \approx 1 \cdot 10^9$. Equation (3) is valid both in the laminar and the turbulent region, however [15].

With data taken from Table I below, Equation (3) can be replaced by the much simpler expression

$$h_{natural} = 307 \cdot (\Delta T)^{0.31} \qquad (5)$$

Figure 2 gives a graphical representation of Eqs. (2), (3), and (5).

The heat transfer coefficients due to forced convection and due to natural convection are not additive; one of them will usually dominate. A simple way to account for this is to merge Eqs. (3) and (5) on the form

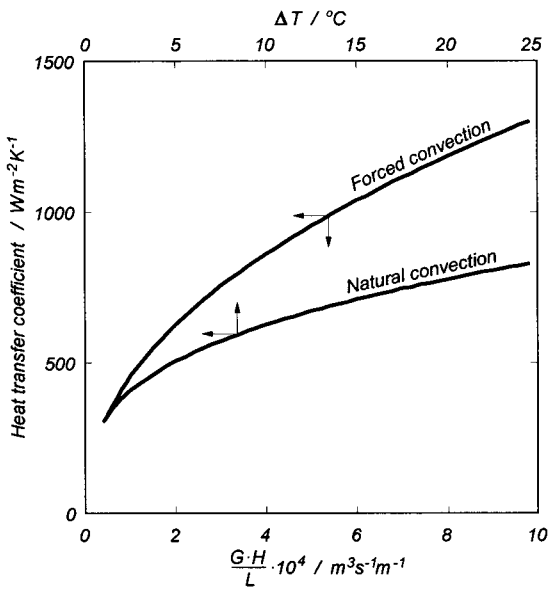

Figure 2. Graphical representation of the heat transfer coefficient between bath and sideledge, calculated from Equation (2) (forced convection) and Eqs. (3) and (5) (natural convection, Eq. (5) probably not visible).

$$h = \left(\left\{ 31480 (G H / L)^{0.46} \right\}^n + \left\{ 307 \cdot \Delta T^{0.31} \right\}^n \right)^{1/n} \qquad (6)$$

where the exponent n is a large number; *e.g.*, $n = 20$ as used in Figure 3. A situation with high superheat and thin ledge (large L) will favour the domination of natural convection.

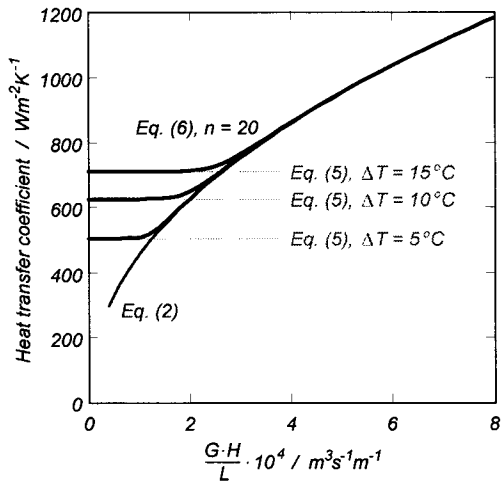

Figure 3. Transition between natural and forced convection (see text).

Dynamic Sideledge Behaviour

Theory

Basic Principles. The sideledge and the bath have different chemical composition. If the sideledge is formed at near equilibrium conditions, it will consist of nearly pure cryolite. This implies that any changes in the ledge thickness must be accompanied by mass transfer as well as by heat transfer (in fact, the terms "precipitation" and "dissolution" could be used, just as well as "freezing" and "melting").

During freezing ("precipitation"), a bath constituent that is not incorporated in the ledge will be enriched at the ledge surface, and it has to diffuse back to the bath. The basic principle was described earlier by Solheim and Støen [20], and it is illustrated in Figure 4.

Multicomponent Diffusion. The bath is a multicomponent mixture containing NaF, AlF_3, Al_2O_3, and CaF_2. The diffusion phenomena must therefore be described using the Stefan-Maxwell equations (*e.g.*, see ref. [15])

$$\nabla x_i = \sum_{j=1}^{n} \frac{1}{c_{tot} D_{ij}} \cdot \left(x_i N_j - x_j N_i \right) \qquad (7)$$

where x_i is the molar fraction of component i, c_{tot} is the total molar concentration [molm^{-3}], D_{ij} (= D_{ji}) is the binary diffusion coefficient for the system i-j [m^{2}s^{-1}], and N is the molar flux [molm^{-2}s^{-1}].

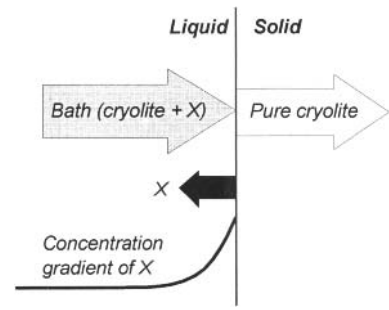

Figure 4. Schematic illustration of fluxes at the surface of the ledge during crystallization of pure cryolite, using the moving surface of the solid as the reference frame. The total (global) flux corresponds to the rate of solid cryolite formation. The total flux of other components than cryolite is zero.

The rate of freezing and the total molar flux N_{tot} are related by

$$N_{tot} = \sum N_i = -\frac{j_{freeze}}{\sum M_i x_{i(s)}} \quad \left[\text{mol m}^{-2}\text{s}^{-1} \right] \qquad (8)$$

where M_i and $x_{i(s)}$ are the molar weight and the molar fraction in the ledge, respectively, of component i. The positive molar flow direction is from the ledge towards the bath, whereas negative values of j_{freeze} means that the ledge is melting away.

For a given rate of freezing the individual molar fluxes are given by the composition of the ledge,

$$N_i = N_{tot} \cdot x_{i(s)} \qquad (9)$$

Turbulent Heat and Mass Diffusivities. In the bulk of the bath, the heat and mass fluxes depend exclusively on convection. Within the boundary layer at the sideledge, the convection decreases gradually and finally becomes zero at the ledge surface, at which point the transport depends only on chemical diffusion and heat conduction. Following the treatment in a previous paper [21], this can be described by using turbulent diffusion coefficients,

$$\text{For mass:} \quad D_{ij} = D_{c(ij)} + D_t \qquad (10)$$

$$\text{For heat:} \quad \alpha = \alpha_c + \alpha_t \quad \text{where} \quad \alpha_c = \lambda / \rho C_p \qquad (11)$$

where D_c is the chemical diffusion coefficient, D_t is the turbulent diffusion coefficient, and α are the corresponding thermal diffusivities of the bath.

The turbulent quantities are zero at the ledge and increase with increasing distance from the ledge (y). Using boundary layer theory, it can be shown that

$$D_t = \alpha_t = C \cdot y^3 \qquad (12)$$

where C is a constant depending only on the degree of convection (*i.e*, a function of the Reynolds number). The mass and heat transfer coefficients, respectively, can then be calculated by

$$k_{(i)} = 0.827 C^{1/3} \cdot D_{c(i)}^{2/3} \qquad (13)$$

and

$$h = 0.827 C^{1/3} \rho C_p \alpha_c^{2/3} \quad (14)$$

where $k_{(i)}$ is the mass transfer coefficient [ms^{-1}] for species *i* in cases where the overall ("global") flux may be neglected. Eq. (14) is derived in the Appendix. It should be noted that the transfer coefficients are proportional to $D^{2/3}$ or $\alpha^{2/3}$ at a given degree of convection (expressed by C), which is in accordance with boundary layer theory.

Numerical Treatment

Main Features of the Model. The numerical calculations were aimed at estimating the bath composition and the local liquidus temperature at the surface of the ledge at a given rate of freezing or melting. The calculations were performed in a spreadsheet, where the region from the ledge and 15 mm into the bath was divided into 1000 equally sized elements. The bath composition was fixed (at "bulk composition") 15 mm from the sideledge.

The numerical procedure involved the shifting between "old" and "new" values of the molar fractions in the discretised version of Equation (7). The procedure produced constant molar fractions after only about 5 iterations, and the operation was performed in an Excel spreadsheet.

Assumptions and Input Data

The physical properties for the bath and the diffusion coefficients are summarized in Table 1. The most uncertain data are probably the diffusion coefficients. For the system $NaF-AlF_3-Al_2O_{3(sat)}$ Burgman and Sides [22] found effective diffusion coefficients for AlF_3 close to $1 \cdot 10^{-8}$ m^2s^{-1}, depending on the NaF/AlF_3 molar ratio. The value $1.5 \cdot 10^{-9}$ m^2s^{-1} for Al_2O_3 in cryolitic melts is based on work by Gerlach *et al.* [23] and Thonstad [24]. The values for binary systems including CaF_2 are little more than surmises.

The heat flow through the ledge (q_l) was fixed at 8000 Wm^{-2}, referred to the ledge surface area. The value of the "convection constant" C in Eqs. (12-14) was fixed at 365 $m^{-1}s^{-1}$, which gives a heat transfer coefficient of 800 Wm^{-2} and s a superheat of 10 °C when the cell is at thermal balance. The density of the sideledge was fixed at 2900 kgm^{-3}.

Table I. Physical data used in the present paper. The bath contains 12 wt% excess AlF_3, 5 wt% CaF_2, and 3 wt% Al_2O_3. The liquidus temperature is 955.2 °C [17] and the superheat was assumed to be 10 °C. The melt was treated as a mixture of NaF (component 1), AlF_3 (2), Al_2O_3 (3) and CaF_2 (4).

Parameter		Value	Ref.
Viscosity [$kgm^{-1}s^{-1}$]		$2.52 \cdot 10^{-3}$	17
Density [kgm^{-3}]		2087	19
Specific heat capacity [$Jkg^{-1}K^{-1}$]		1883	18
Heat of melting [$kJkg^{-1}$]		502.3	18
Thermal conductivity [$Wm^{-1}K^{-1}$]		0.795	13
Diffusion coefficients [m^2s^{-1}]	D_{12}	$1.0 \cdot 10^{-8}$	22
	D_{13}	$1.5 \cdot 10^{-9}$	23, 24
	D_{14}	$3.0 \cdot 10^{-9}$	-
	D_{23}	$1.5 \cdot 10^{-9}$	23, 24
	D_{24}	$3.0 \cdot 10^{-9}$	-
	D_{34}	$1.5 \cdot 10^{-9}$	-

Results

Temperature Gradients. Some calculated temperature gradients are shown in Figure 5. During freezing, AlF_3, CaF_2, and Al_2O_3 become more concentrated near the ledge, and the liquidus temperature decreases. During melting, the concentrations of bath constituents other than cryolite decrease, and the liquidus temperature increases correspondingly. It follows that the "superheat" measured in specialized *in situ* sensors [25] in no way should be taken to represent the difference between the bath temperature and the surface temperature of the sideledge. Unexpected high or low measured "superheats" may indicate that the sideledge is either melting away or freezing during the time of measurement.

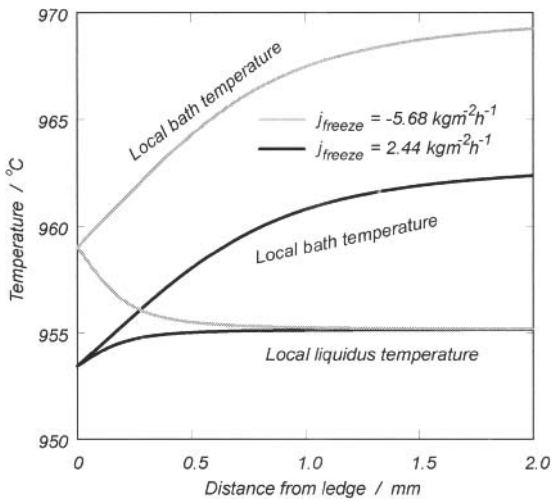

Figure 5. Temperature gradients close to the ledge. Grey curves – during melting (-1.96 mm/h), black curves – during freezing (0.84 mm/h). It was assumed that the sideledge consists of pure cryolite.

Limit for Formation of Pure Cryolite. If one assumes that pure cryolite is the only solid phase formed, the area close to the ledge will be supercooled if the rate of freezing is high enough. This is related to the fact that the thermal boundary layer (which determines the course of the local actual temperature) is thicker than the diffusion layer (which determines the course of the local liquidus temperature). The supercooling will increase with increasing distance from the surface, which favours dendritic crystal growth. In that case, pure cryolite will not longer be formed, since bath will be "trapped" between the dendrites. The criterion for formation of pure cryolite is, obviously,

$$\left.\frac{dT_b}{dy}\right|_{y=0} \geq \left.\frac{dT_{liq}}{dy}\right|_{y=0} \quad (15)$$

With the present data and assumptions, the onset of dendrite formation was found to take place at a freezing rate as low as 1.13 mm/h (3.28 $kgm^{-2}h^{-1}$).

Composition of Freeze. Dendritic crystal growth during rapid freezing was simulated by adjusting the flow (N) of each bath constituent in such a way that $dT_b/dy = dT_{liq}/dy$ (see Eq. (16)); at

the same time, there should be agreement between the rate of freezing and the heat flow. From the calculated flow, the composition of the ledge could be computed, as shown in Figure 6. The cell is at thermal balance when the superheat (defined as the difference between the actual temperature and the liquidus temperature for the bulk) is 10 °C. If the superheat is above 7 °C, pure cryolite, or a solid solution containing small amounts of AlF_3 and CaF_2, is formed. If the superheat drops below 7 °C, the contents of AlF_3, CaF_2, and Al_2O_3 in the ledge start to increase abruptly. It is interesting to note that the change from "almost pure cryolite" to "almost bath composition" takes place in a very narrow temperature range, which may explain the alternating distinct bands of needle-shaped crystals and disordered or even porous structures observed in samples of industrial sideledge [20].

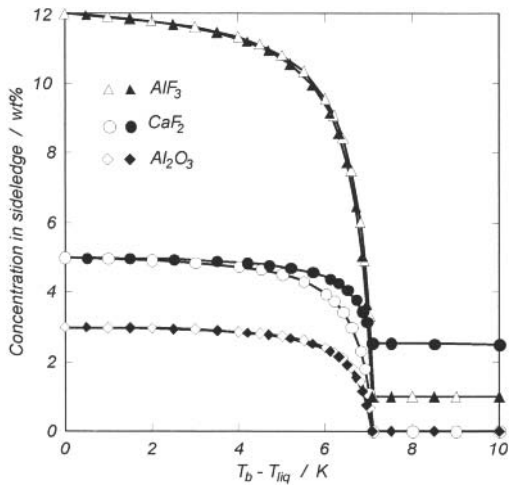

Figure 6. Composition of the sideledge as a function of the superheat. Open symbols – no solid solubility of CaF_2 in cryolite, filled symbols – assumed 2.5 wt% solid solubility of CaF_2 in cryolite. It was assumed that the solid solubility of AlF_3 is 1 wt%.

Rate of Freezing and Melting. The rate of freezing and melting is normally calculated by

$$j_{freeze} = \frac{q_{sl} - h \cdot (T_b - T_{liq})}{\Delta H_m} \quad [kgm^{-2}s^{-1}] \qquad (16)$$

where q_{sl} is the heat flow from the ledge surface and out of the cell, and ΔH_m is the heat of melting. As will be clear from the treatment above, however (*e.g.*, Figure 5), the surface temperature equals the liquidus temperature only at thermal balance.

The numerical calculations indicated that the ledge surface temperature (T^*) varies linearly with the rate of freezing or melting, at least when the rates are small. Furthermore, according to the Chilton-Colburn analogy [15] the mass transfer coefficients vary linearly with the heat transfer coefficient. Consequently, one would expect that the concentration difference between bulk and surface, and hence, the difference between T^* and T_{liq}, is inversely proportional to the heat transfer coefficient. This gives

$$T^* = T_{liq} - \frac{j_{freeze}}{h} \cdot f(x_{melt}, x_{solid}) \qquad (17)$$

where the function f, which comprises the bath and ledge compositions, must be determined by numerical treatment. By replacing T_{liq} by T^* in Eq. (16), followed by inserting Eq. (17) into (16), one obtains

$$j_{freeze} = \frac{q_{sl} - h\,(T_b - T_{liq})}{\Delta H_m \cdot CF} \quad \text{where}$$
$$CF = 1 + \frac{f(x_{melt}, x_{solid})}{\Delta H_m} \qquad (18)$$

In cases where the bath and the sideledge have the same composition, the correction factor CF will be unity and Eq. (16) applies, since there will be no concentration gradients near the ledge.

A large number of numerical calculations were made in order to assess CF. A reasonable fit was obtained by using the function

$$j_{freeze} = \frac{q_{sl} - h\,(T_b - T_{liq})}{\Delta H_m \cdot \left[1 + 0.2 \cdot \left(\sum c_{bath} - \sum c_{ledge}\right)\right]} \quad [kgm^{-2}s^{-1}] \qquad (19)$$

where c are concentrations in weight percent of other bath components than cryolite in the bath and in the ledge.

Figure 7 shows a comparison between Eq. (16) and Eqs. (18)-(19), using randomised variables (AlF_3, CaF_2, and Al_2O_3 concentrations in bath and ledge, heat flow, heat transfer coefficient, and superheat). As can be observed, Eq. (19) generally agrees much better with the numerical data, especially at low and moderate rates, and it predicts lower rates of freezing and melting than the traditional Eq. (16). This agrees with the work by Rye *et al.* [25], who studied the ledge behaviour in industrial cells; citation: "*Results indicate that the melting of the frozen ledge* [during anode effect] *may be less severe than predicted by thermal models.*"

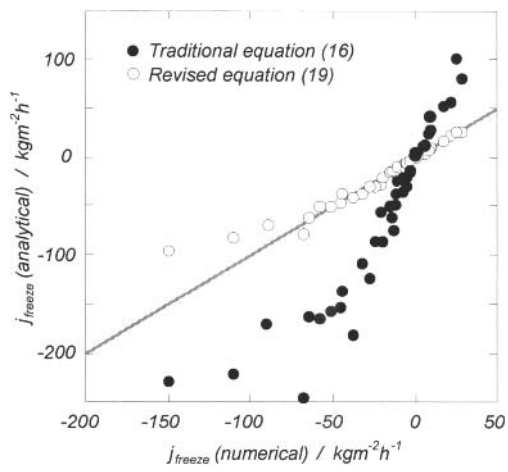

Figure 7. Rate of freezing or melting; comparison between Eqs. (16) and (19) and numerical results, using randomised input data. The straight line represents the "ideal" relationship.

Acknowledgement

The present work was financed by Hydro Primary Metal Technology. Permission to publish the results is gratefully acknowledged. The author wants to thank colleagues at SINTEF and in Hydro for discussions and suggestions during the preparation of this paper. Special thanks to Nancy Holt, Hydro PMT, for initiating this work.

References

1. A. Korobov and E.A. Yanko, "Pecularities in the Convective Heat Transfer by the Smelt in Aluminium Converters of High Capacity", Publication of the VAMI Institute #60, Leningrad, 1967.
2. E. Haupin, "Calculating Thickness of Containing Walls Frozen from Melt", *J. Metals* **23** (July), 41 (1971).
3. Arai and K. Yamazaki, "Heat Balance and Thermal Losses in Advanced Prebaked Anode Cells, Light Metals 1975, Vol. 1, p. 193.
4. Y. Arita, N. Urata, and H. Iteuchi, "Estimation of Frozen Bath Shape in an Aluminium Reduction Cell by Computer Simulation", Light Metals 1978, Vol. 1, p. 59.
5. H. Ikeuchi and Y. Arita, "Treatment of Freeze-Melt Boundary Layer in Aluminium Reduction Cell", *Yoyven* **21** (2) 215 (1978).
6. J.G. Peacey and G.W. Medlin, "Cell Sidewall Studies at Noranda Alumium", Light Metals 1979, p. 475.
7. A. Solheim and J. Thonstad, "Model Experiments of Heat Transfer Coefficients between Bath and Side Ledge in Aluminium Cells", *J. Metals* **36** (3) 51 (1984). (Also in Light Metals 1983, p. 425.
8. T. Ohta and T. Matsushima, "Thermal Analysis of Soederberg Pots", Light Metals 1984, p. 689.
9. M.P. Taylor and B.J. Welch, "Bath/Freeze Heat Transfer Coefficients: Experimental Determination and Industrial Application", Light Metals 1985, p. 781.
10. K.J. Fraser, M.P. Taylor, and A.M. Jenkin, "Bath Heat Transfer and Mass Transport Processes in H-H Cells, Light Metals 1990, p. 221.
11. Y.R. Gan and J. Thonstad, "Heat Transfer Between Molten and Solid Cryolite Bath", Light Metals 1990, p. 421.
12. A. Warczok, T. Utigard, and P. Descleaux, "Heat Transfer Between Molten Cryolite and Solid Phase", Savard/Lee International Symposium on Bath Smelting", Montreal, Quebec, Canada, October 18-22, 1992 (Proceedings, p. 325).
13. V.A. Khoklov, E.A. Filatov, A. Solheim, and J. Thonstad, "Thermal Conductivity in Cryolitic Melts - New Data and Its Influence on Heat Transfer in Aluminium Cells", Light Metals 1998, p. 501.
14. K. Bech, S. T. Johansen, A. Solheim, and T. Haarberg, "Coupled Current Distribution and Convection Simulator for Electrolysis Cells", Light Metals 2001, p. 463.
15. J.T. Welty, C.E. Wicks, and R.E. Wilson, Fundamentals of Momentum, Heat, and Mass Transfer, 3rd edition, John Wiley & Sons, 1984.
16. T. Herzberg, K. Tørklep, and H.A. Øye, "Viscosity of Molten NaF-AlF_3-Al_2O_3-CaF_2 Mixtures", Light Metals 1980, p. 159.
17. A. Solheim, S. Rolseth, E. Skybakmoen, L. Støen, Å. Sterten, and T. Støre, "Liquidus Temperatures for Primary Crystallization of Cryolite in Molten Salt Systems of Interest for the Aluminium Electrolysis", *Met. Trans. B*, **27B** 739 (1996).
18. M.V. Chase *et al.*, JANAF Thermochemical Data (*J. Phys. Chem. Ref. Data*, Vol. 14, Suppl. 1, 1985).
19. A. Solheim, "The Density of Molten NaF-LiF-AlF_3-CaF_2-Al_2O_3 in Aluminium Electrolysis", *Aluminum Transactions* **2** (1) (2000), p. 161.
20. A. Solheim and L.I.R. Støen, "On the Composition of Solid Deposits Frozen out from Cryolitic Melts", Light Metals 1997, p. 325.
21. A. Solheim, "Crystallization of Cryolite and Alumina at the Metal-Bath Interface in Aluminium Reduction Cells", Light Metals 2002, p. 225.
22. J.W. Burgman and P.J. Sides, "Measurement of Effective Diffusivity in Hall/Heroult Electrolytes", Light Metals 1988, p. 673.
23. J. Gerlach, U. Hennig und H.-D. Pöthsch, "Zur Auflösungskinetik von Aluminiumoxid in Kryolithschmelzen mit Zusätzen von Al_2O_3, AlF_3, CaF_2, LiF oder MgF_2, *Erzmetall*, **31** 496 (1978).
24. J. Thonstad, "Chronopotentiometry Measurements on Graphite Anodes in Cryolite-Alumina Melts", *Electrochim. Acta*, **14** 127 (1969).
25. K.Å. Rye, T. Eidet, and K. Tørklep, "Dynamic Ledge Response in Hall-Heroult Cells", Light Metals 1999, p. 347.

Appendix: Derivation of Heat Transfer Coefficient from Turbulent Thermal Diffusivity

The heat flow in the boundary layer next to the sideledge can be expressed by

$$q = -\rho C_p(\alpha_c + \alpha_t)\cdot\frac{dT}{dy} \qquad \left[W\,m^{-2}\right] \tag{A1}$$

where q is formally negative when heat is flowing from the bath to the sideledge. Assuming that the turbulent thermal diffusivity close to the sideledge varies as

$$\alpha_t = C\cdot y^3 \qquad \left[m^2 s^{-1}\right] \tag{A2}$$

the above equations combine to give

$$dT = -\frac{q}{C\cdot\rho C_p}\cdot\frac{dy}{\beta^3 + y^3} \quad \text{where } \beta = \left(\frac{\alpha_c}{C}\right)^{1/3} \tag{A3}$$

The temperature profile near the ledge can be found by integrating Eq. (A3) from y = 0 to a distance y from the ledge surface,

$$T_y = T_l - \frac{q}{C\cdot\beta^2\cdot\rho C_p}\left\{\frac{1}{6}\cdot\ln\left(\frac{(\beta+y)^3}{\beta^3+y^3}\right) + \frac{1}{\sqrt{3}}\cdot\tan^{-1}\left(\frac{2y-\beta}{\sqrt{3}\beta}\right) + \frac{\pi}{6\sqrt{3}}\right\} \tag{A4}$$

For very large y, we obtain

$$T_b - T_l = \frac{2\pi}{3\sqrt{3}}\cdot\frac{q}{\rho C_p \alpha_c^{2/3}\cdot C^{1/3}} \tag{A5}$$

and the heat transfer coefficient becomes

$$h = \frac{q}{T_b - T_l} = 0.8270\rho C_p \alpha_c^{2/3} C^{1/3} \tag{A6}$$